Structure and magnetism of new hybrid cobalt hydroxide materials built from decorated brucite layers†

Tony D. Keene,[a,c] Mark E. Light,[b] Michael B. Hursthouse[b] and Daniel J. Price*[a]

[a] *WestCHEM, School of Chemistry, University of Glasgow, Glasgow, G12 8QQ, United Kingdom. E-mail: Daniel.Price@glasgow.ac.uk; Fax: +44-141-330-4888*
[b] *School of Chemistry, University of Southampton, Highfield, Southampton, SO17 1BJ, United Kingdom.*
[c] *Present address: School of Chemistry, Building F11, The University of Sydney, Sydney, NSW 2006, Australia.*

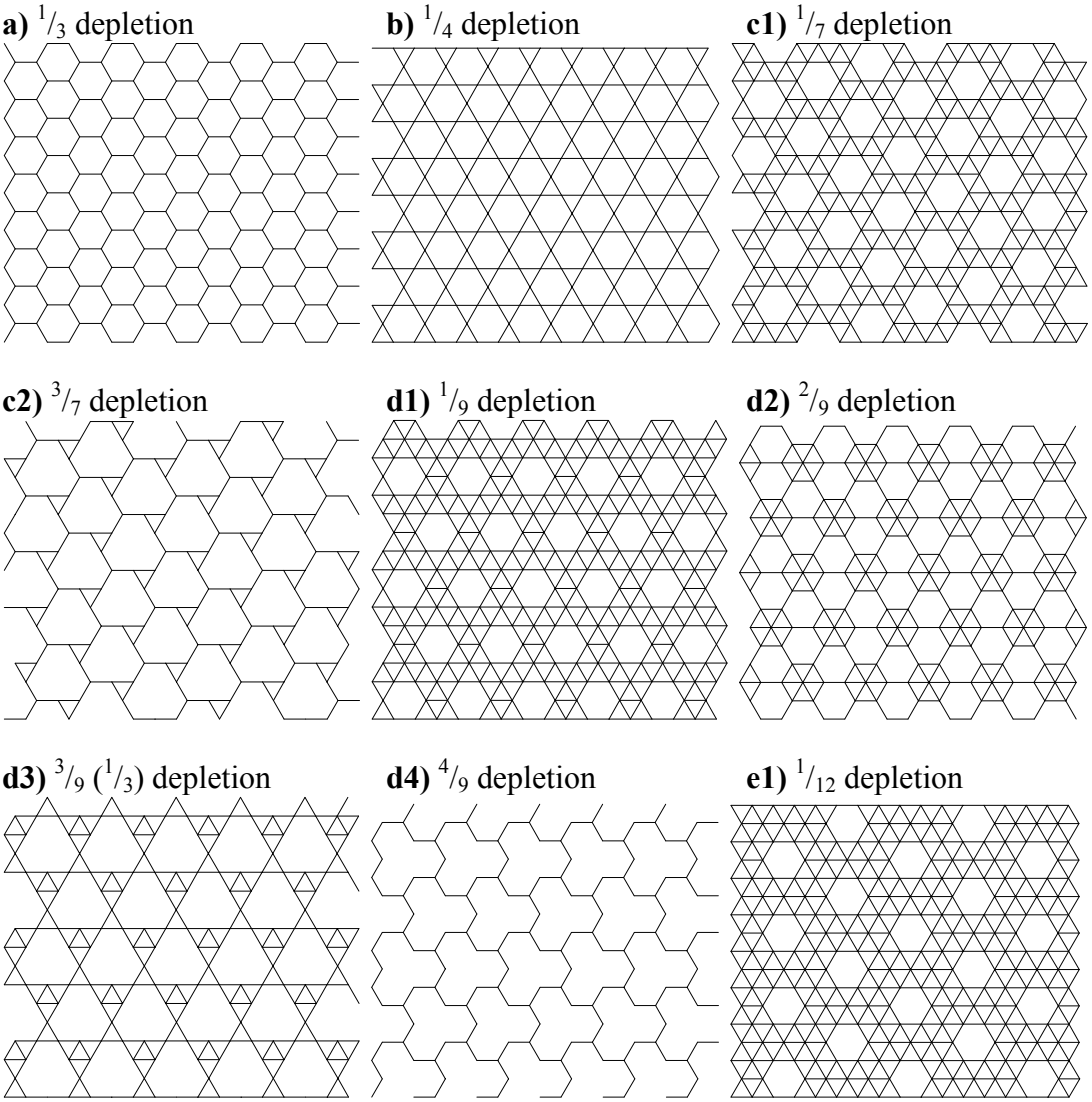

e2) $^{2}/_{12}$ ($^{1}/_{6}$) depletion

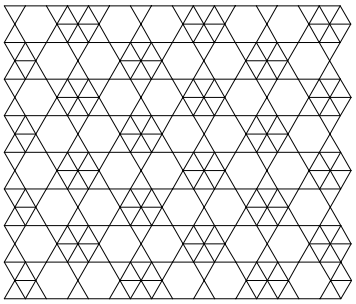

e3) $^{3}/_{12}$ ($^{1}/_{4}$) depletion

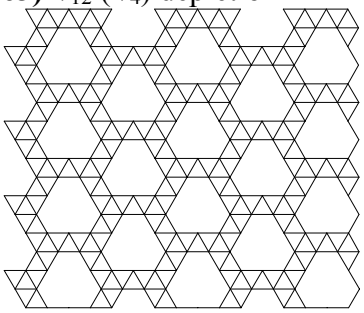

e4) $^{3}/_{12}$ ($^{1}/_{4}$) depletion

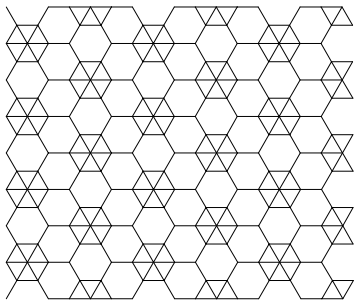

e5) $^{4}/_{12}$ ($^{1}/_{3}$) depletion

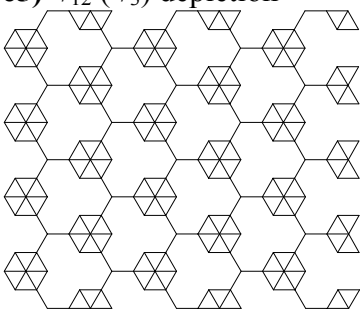

e6) $^{5}/_{12}$ depletion

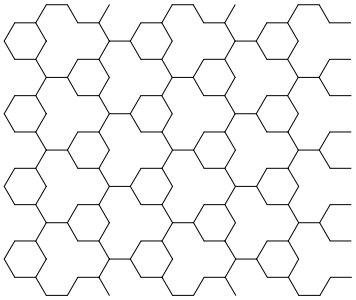

e7) $^{6}/_{12}$ ($^{1}/_{2}$) depletion

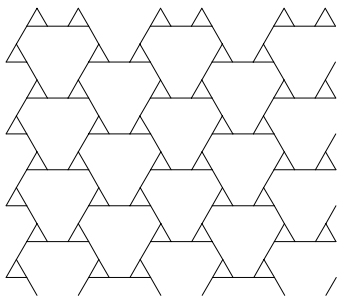

f1) $^{1}/_{13}$ depletion

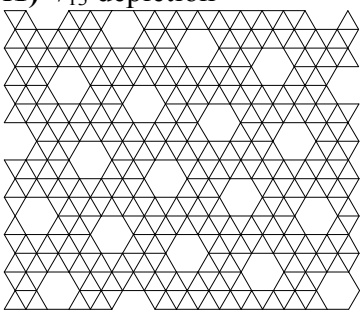

f2) $^{3}/_{13}$ depletion

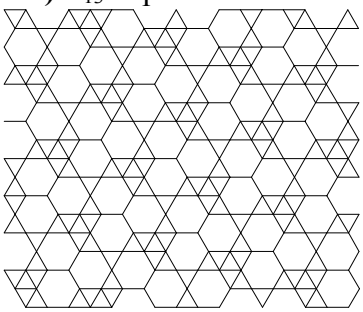

f3) $^{3}/_{13}$depletion

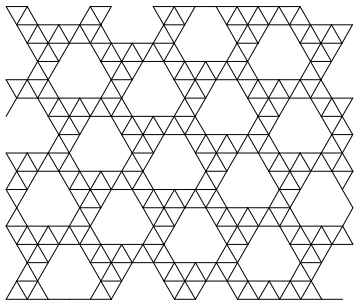

f4) $^{4}/_{13}$ depletion

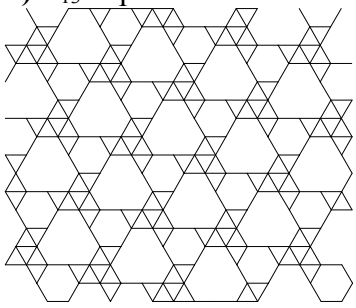

f5) $^{4}/_{13}$ depletion

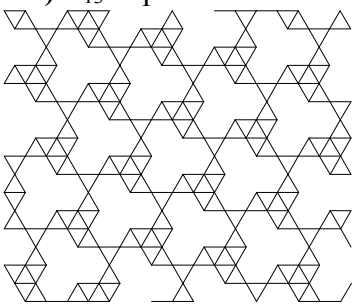

f6) $^{6}/_{13}$ depletion

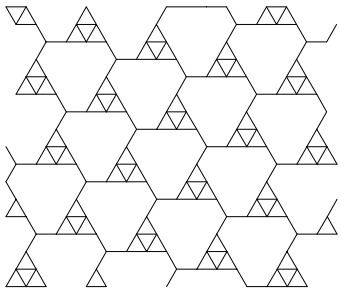

f7) $^{7}/_{13}$ depletion

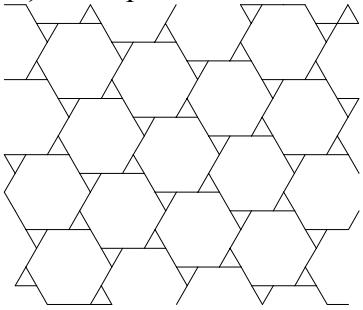

g1) $^{1}/_{16}$ depletion

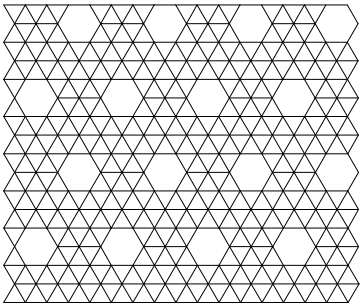

g2) $^{3}/_{16}$ depletion

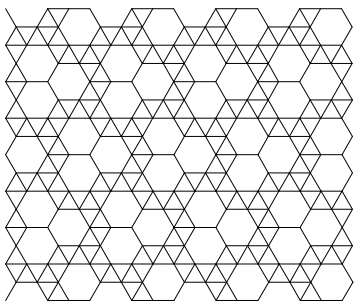

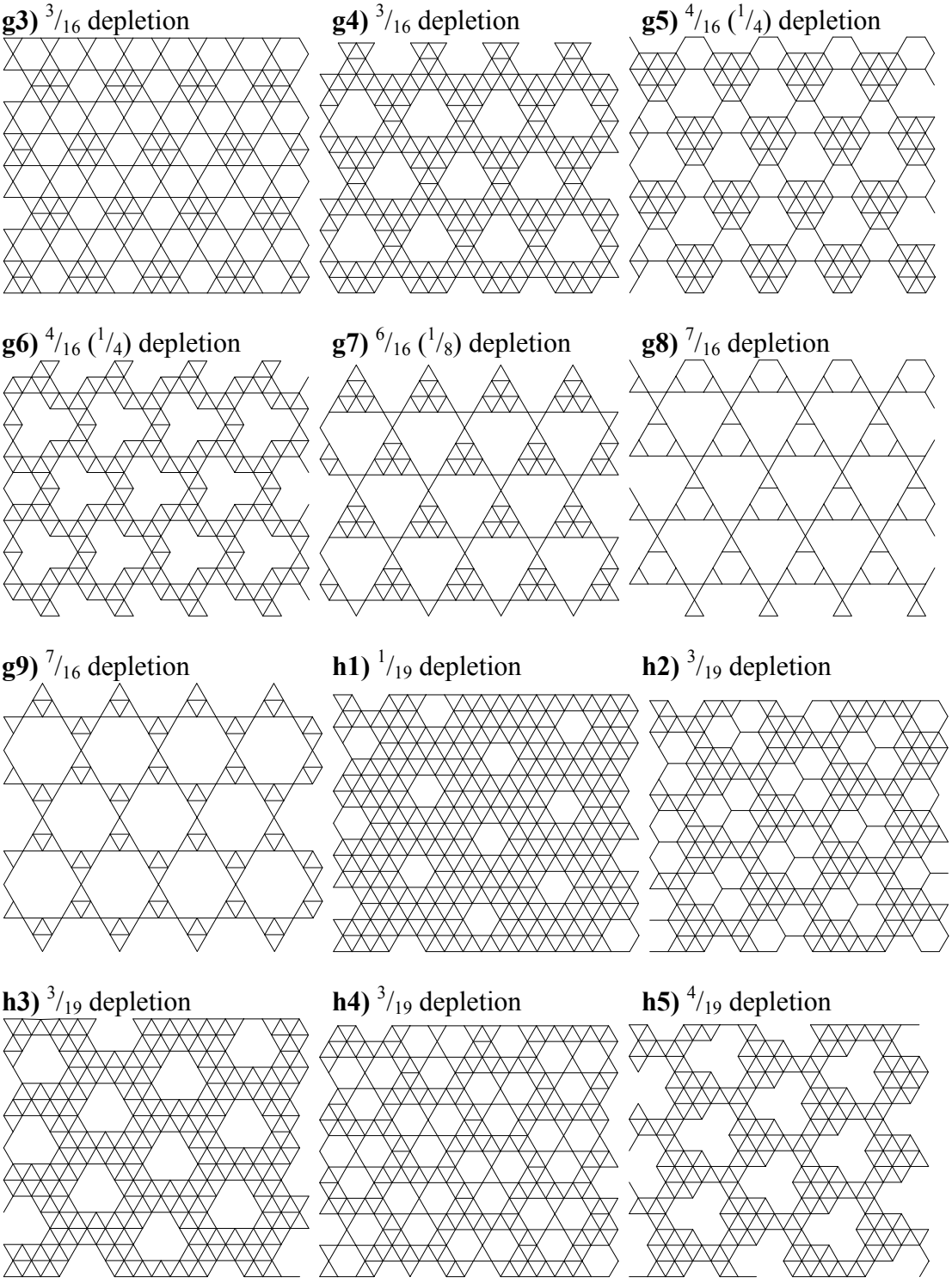

Figure S1. Possible trigonally symmetric lattices derived via periodic site depletion of a triangular lattice. Only certain fractions can support such a trigonal symmetry, and the series starts: $^{1}/_{3}$, $^{1}/_{4}$, $^{1}/_{7}$, $^{1}/_{9}$, $^{1}/_{12}$, $^{1}/_{13}$, $^{1}/_{16}$, $^{1}/_{19}$, . . . Some of these networks are very common such as the honeycomb net **a)** which has a great many physical realisations. The network **b)** is also known as the kagomé lattice, and is the maximally topologically frustrated 2-D net. The $^{1}/_{7}$ depleted net **c1)**, is also known as the maple leaf lattice, and provides a link between the 3-connected kagomé net and the 6-connected triangular lattice. The compounds presented here have structures based upon **d1)** the $^{1}/_{9}$ depleted net and **h2)** the $^{3}/_{19}$ depleted net.

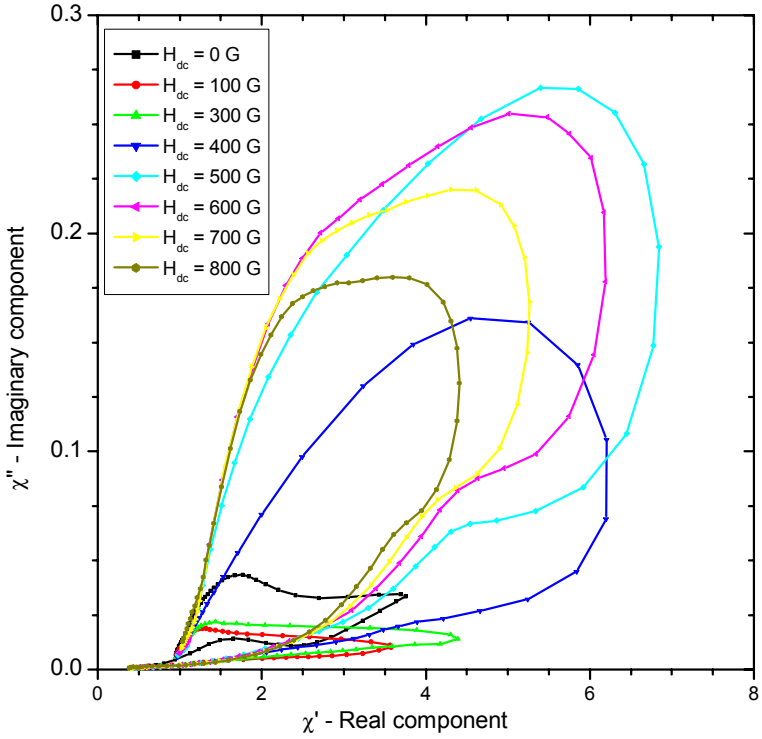

Figure S2. Dynamic aspect of the magnetic susceptibility of **1**. A plot derived from the a.c. susceptibility measurements where the imaginary component is plotted against the real component. $H_{a.c.}$ = 3.5 G, drive frequency ω = 103 Hz, measurements were performed on a powder sample of **1**, as a function of d.c. offset field ($H_{d.c.}$ = 0 – 800 G). Each curve corresponds to a temperature sweep; (5 – 40 K). Such a plot is often described as a Cole-Cole plot and is used to look at simple relaxation processes. In this case the very complex shape is evidence of much more complex magnetism, and cooperativity associated with magnetically ordered phases.

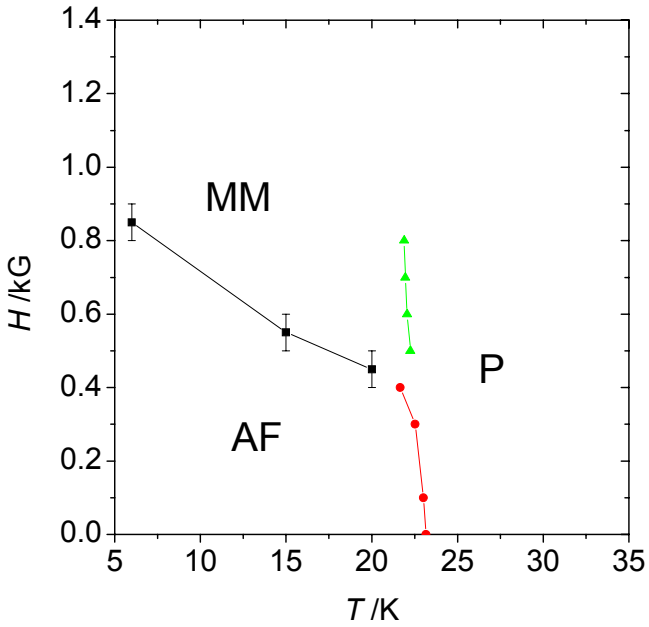

Figure S3. Semi-quantitative magnetic phase diagram for **1**, for H parallel to the crystallographic *c*–axis. P – paramagnetic state; AF – antiferromagnetically ordered state; MM – metamagnetic state. Phase boundaries are determined from isothermal (AF – MM) and isofield d.c. magnetisation measurements, (P – AF) and (P – MM) transitions from a.c. susceptibility measurements. Although the data taken form a microcrystalline bulk powder sample, the magnetisation data is dominated by the components when field H, is parallel to the *c*-axis.

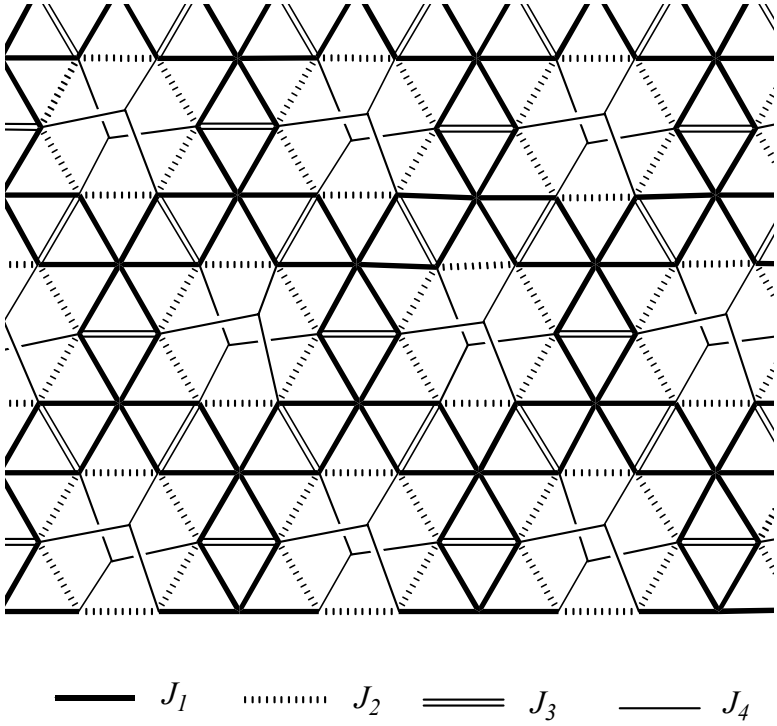

Figure S4. Showing the hydroxyl mediated spin coupling interactions within the $[Co_{10}(OH)_{18}]_n^{2n+}$ 2-D network of **1**, derived from the $^1/_9$ depleted decorated triangular lattice.

Table S1: Possible coupling interactions in 1: The four interactions can either be ferromagnetic (+) or antiferromagnetic (–), resulting in 16 possible spin configurations for the layer.

Configuration	J_1	J_2	J_3	J_4	*Net layer magnetisation*
a	+	+	+	+	10Co, no frustration
b	+	+	+	–	6Co, no frustration
c	+	+	–	+	Frustration
d	+	+	–	–	Frustration
e	+	–	+	+	Frustration
f	+	–	+	–	Frustration
g	+	–	–	+	Frustration
h	+	–	–	–	Frustration
i	–	+	+	+	6 Co, no frustration
j	–	+	+	–	2 Co, no frustration
k	–	+	–	+	Frustration
l	–	+	–	–	Frustration
m	–	–	+	+	Frustration
n	–	–	+	–	Frustration
o	–	–	–	+	Frustration
p	–	–	–	–	Frustration

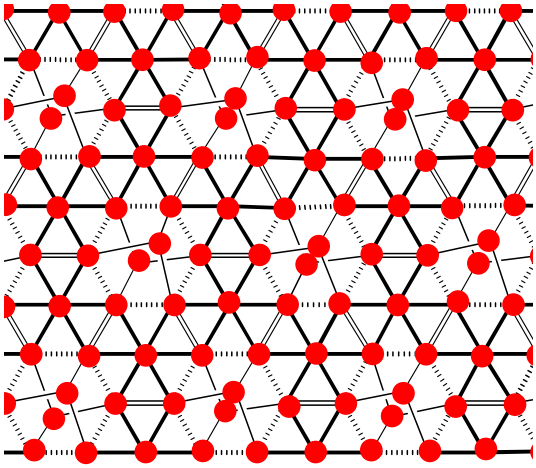

Spin configuration *a*: + + + +

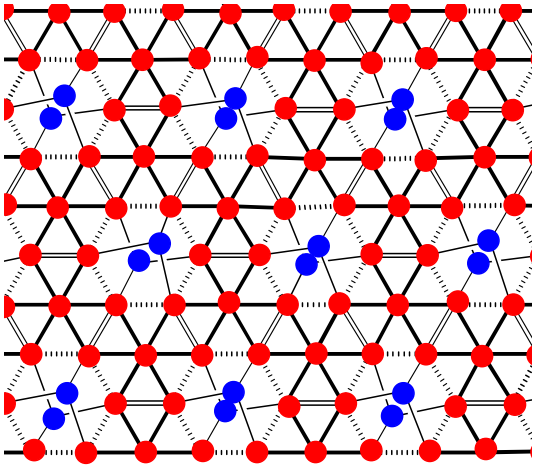

Spin configuration *b*: + + + –

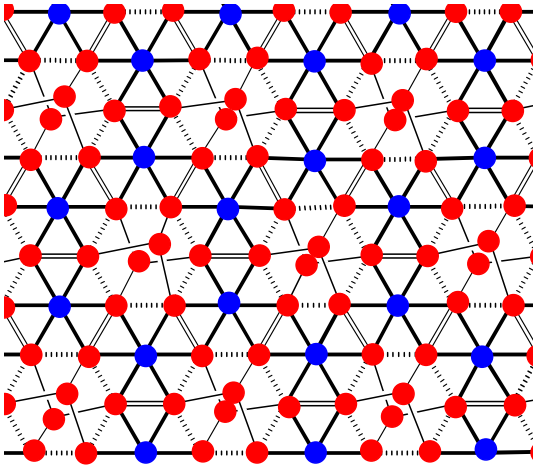

Spin configuration *i*: – + + +

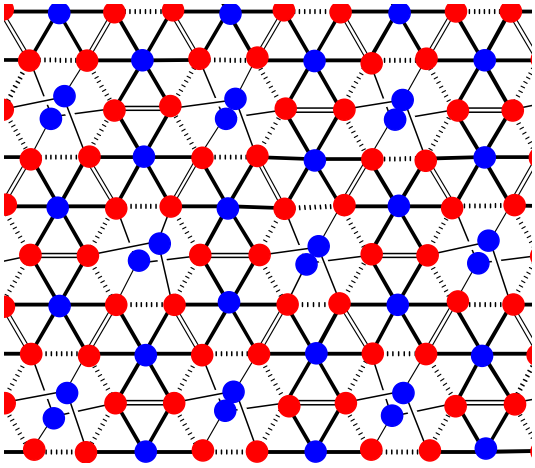

Spin configuration *j*: – + + –

Figure S5. Showing the relative spin orientations for the non-frustrated coupling schemes in **1**; *a*, *b*, *i*, *j* (as labelled in Table S1). Red – spin up; blue – spin down.

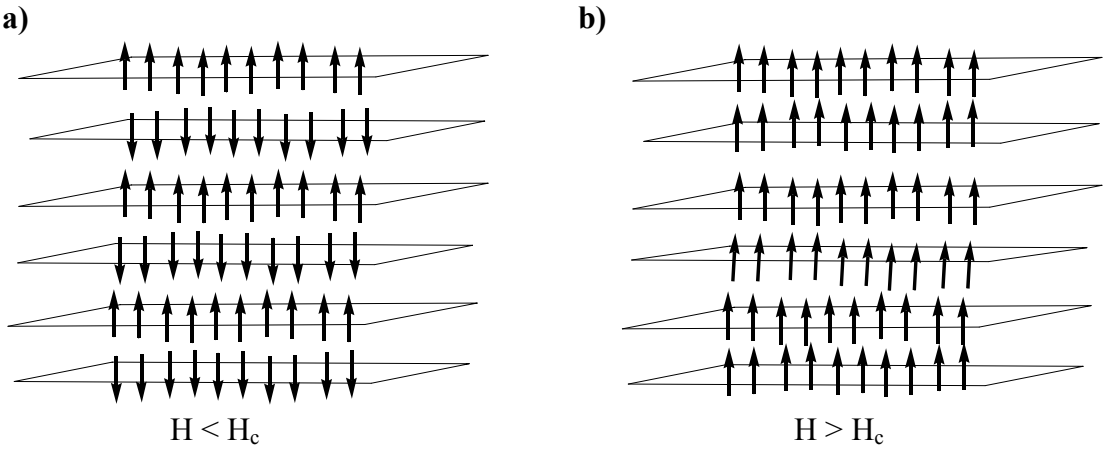

Figure S6. Schematic showing the relationship between the antiferromagnetic ground state in **1 a)** in which ferromagnetic layers are coupled by a weak antiferromagetic interlayer interaction. **b)** Above a critical field H_c, we observe a transition to a state with a much higher magnetisation, in which the weak interlayer coupling is overcome, and neighbouring layers have a parallel alignment.

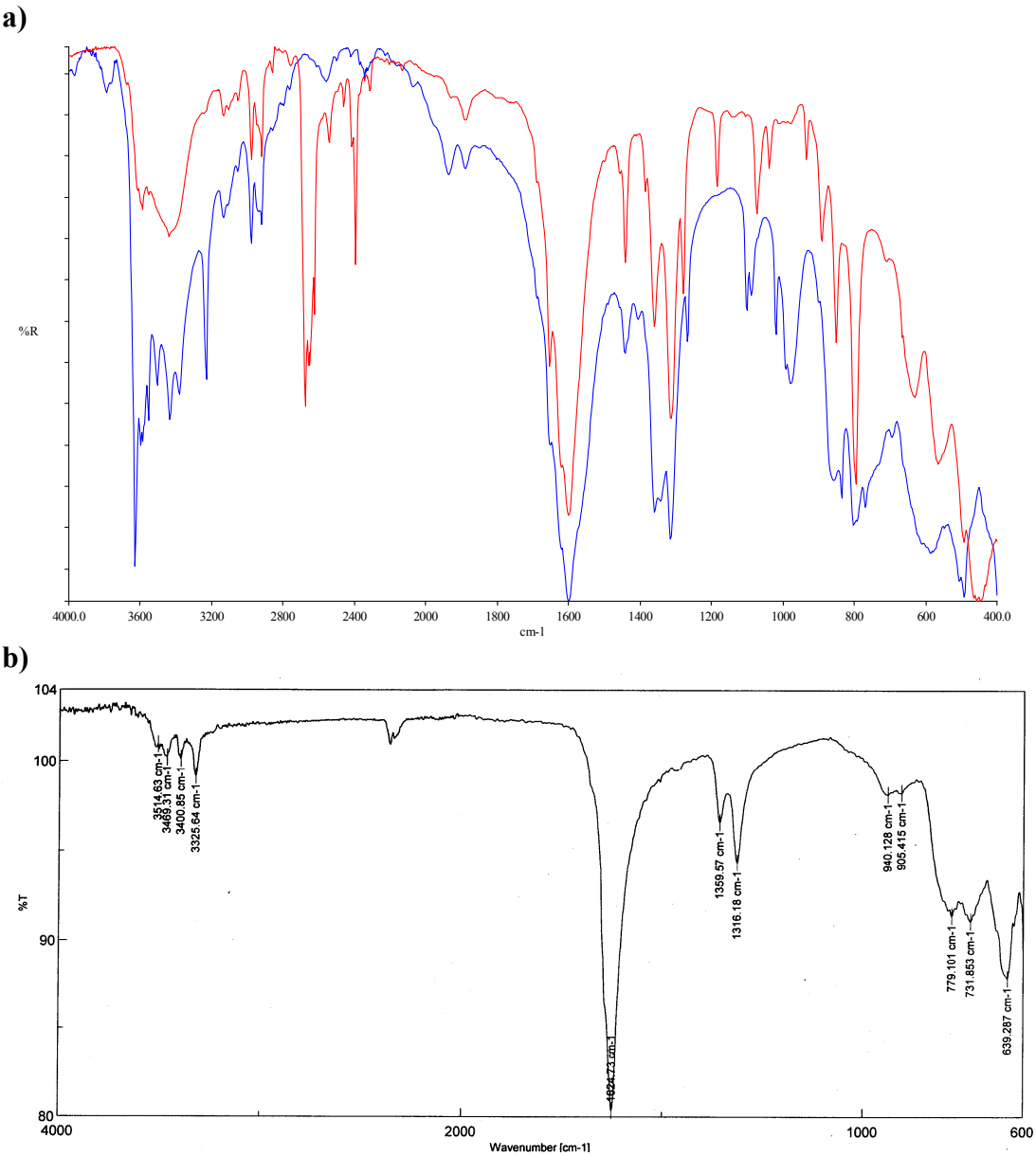

Figure S7. FT-ATR infrared spectra. **a)** Compound **1**. Hydrogenous material - blue line, and the partially deuterated compound - red line. **b)** Compound **3** as a hydrogenous form.

Crystallographic Information Files

Crystallographic data has been deposited with the CSD; CCDC references numbers 275122 (**1**), 275671 (**2**) and 219800 (**3**).